Journal of Radiation Research, 2013, 54, 736–747
doi: 10.1093/jrr/rrs132 Advance Access Publication 3 January 2013

SPICE-NIRS Microbeam: a focused vertical system for proton irradiation of a single cell for radiobiological research

Teruaki KONISHI[1,*], Masakazu OIKAWA[1], Noriyoshi SUYA[1], Takahiro ISHIKAWA[1], Takeshi MAEDA[1], Alisa KOBAYASHI[1], Naoko SHIOMI[1], Kumiko KODAMA[1], Tsuyoshi HAMANO[2], Shino HOMMA-TAKEDA[3], Mayu ISONO[1,4], Kotaro HIEDA[5], Yukio UCHIHORI[1] and Yoshiyuki SHIRAKAWA[1]

[1]Research Development and Support Center, National Institute of Radiological Sciences, 4-9-1 Inage-ku, Chiba-shi 263-8555, Japan
[2]Research Center for Radiation Emergency Medicine, National Institute of Radiological Sciences, 4-9-1 Inage-ku, Chiba-shi 263-8555, Japan
[3]Research Center for Radiation Protection, National Institute of Radiological Sciences, 4-9-1 Inage-ku, Chiba-shi 263-8555, Japan
[4]Graduate School of Human Health Sciences, Metropolitan University of Tokyo, 7-2-10 Higashi-ogu, Arakawa-ku, Tokyo116-8551, Japan
[5]Department of Life Science, College of Science, Rikkyo University, 3-34-1 Nishi-Ikebukuro, Toshima-ku, Tokyo 171-8501, Japan
*Corresponding author. Tel: +81-43-206-4695; Fax: +81-43-206-3514; E-mail: tkonishi@nirs.go.jp

(Received 1 October 2012; revised 4 December 2012; accepted 4 December 2012)

The Single Particle Irradiation system to Cell (SPICE) facility at the National Institute of Radiological Sciences (NIRS) is a focused vertical microbeam system designed to irradiate the nuclei of adhesive mammalian cells with a defined number of 3.4 MeV protons. The approximately 2-μm diameter proton beam is focused with a magnetic quadrupole triplet lens and traverses the cells contained in dishes from bottom to top. All procedures for irradiation, such as cell image capturing, cell recognition and position calculation, are automated. The most distinctive characteristic of the system is its stability and high throughput; i.e. 3000 cells in a 5 mm × 5 mm area in a single dish can be routinely irradiated by the 2-μm beam within 15 min (the maximum irradiation speed is 400 cells/min). The number of protons can be set as low as one, at a precision measured by CR-39 detectors to be 99.0%. A variety of targeting modes such as fractional population targeting mode, multi-position targeting mode for nucleus irradiation and cytoplasm targeting mode are available. As an example of multi-position targeting irradiation of mammalian cells, five fluorescent spots in a cell nucleus were demonstrated using the γ-H2AX immune-staining technique. The SPICE performance modes described in this paper are in routine use. SPICE is a joint-use research facility of NIRS and its beam times are distributed for collaborative research.

Keywords: microbeam; proton; vertical beam; single hit; target irradiation; bystander effect; low dose effect

INTRODUCTION

There is continuing interest in the use of microbeam irradiation systems designed to deliver a defined number of charged particles on a single cell with a resolution of a few micrometres. Irradiation of an exact number of charged particles on a single cell means that the limitations of the Poisson distribution of the number of charged particles can be overcome. This is especially important in low-dose regions because a small number of charged particles per cell will inevitably lead to large fluctuations in the cell population in a broad-beam irradiation field. Moreover, microbeams are particularly useful in the field of radiation-induced bystander effects, an important phenomenon in low-dose effects [1, 2]. In addition, microbeams with beam sizes of less than a few micrometres enable us to irradiate a desired site within the cell.

The earliest experiments employing single-cell microbeam irradiation with accelerated charged particles were performed in the 1950s [3]. Radiation biology using microbeam irradiation techniques has been advanced remarkably by the successful development of the proton and helium ion microbeams at Gray Cancer Institute and Columbia University in the 1990s [4–6]. These two microbeam facilities adopted collimation systems with a capillary or a pair of apertures and successfully produced 5- to 10-μm diameter beams. Such beam sizes are almost the lower limit for a collimator-based microbeam of light ions, and thus microbeams focused with electrostatic/magnetic lenses have been developed to reduce the diameter of the beam. In addition to beam size, another important feature of microbeams for radiobiological studies is the orientation of the beam line, either horizontal or vertical. A vertical beam has an advantage over a horizontal beam in that a cell dish can be set on the micro-positioning stage in its natural orientation and held there with a simple holder, allowing cells to be maintained in an optimal environment that minimizes cell stress. At present, many charged particle microbeam facilities equipped with focusing or collimation have been established and are operational [7–10]. Several proton microbeam facilities provide vertical beams of less than a few micrometres in diameter. Microbeam II of Radiological Research Accelerator Facility at Columbia University achieves an upward vertical beam with a submicrometre beam diameter by electrostatic quadrupole triplet lenses, and the current overall irradiation throughput is about 10 000 cells/h [7, 8]. The microbeam facility at Physikalisch-Technische Bundesanstalt (PTB) provides downward vertical beams with a diameter of a few micrometres, and the overall experimental speed is 50 000 cells/h by using an electrostatic beam scanner [12]. Recently, the Surrey vertical microbeam facility was reported as a new facility that provides an upward vertical microbeam of ions from protons to calcium with a diameter of a few micrometres [13]; however, mammalian cells were irradiated with a time-controlled method, and thus the precise number of irradiated particles is unknown. In this paper, we describe the current status and performance of the proton microbeam irradiation system named the Single Particle Irradiation system to Cell (SPICE) at the National Institute of Radiological Sciences (NIRS). SPICE provides a 3.4-MeV proton microbeam focused with a quadrupole magnetic lens on an upward vertical beam line. The construction of the prototype of SPICE began in 2003 with the primary goal of targeting 2000 cells/h with a 2-μm diameter proton microbeam [14]. After improving the vertical beam line structures and accelerator stability, a beam size of 10 μm was obtained in 2006 [15]. After further optimization of the beam focusing system and improvements in the stability of the bending magnets, the beam size was reduced to approximately 5 μm. In 2008, an automated cell recognition system for targeting cell nuclei in a 2.5 mm × 2.5 mm area of the cell dish was also completed [16]. Now, after additional improvements, SPICE provides a beam size of approximately 2 μm in diameter and its irradiation procedures are fully automated with high-throughput irradiation of 3000 cells in a 5 mm × 5 mm area in a single dish within 15 min after placing the cell dish on the micro-positioning stage. At present, SPICE is the only proton microbeam facility at which a single-ion single-cell irradiation can be performed on mammalian cells with stability and high throughput by using an upward vertical beam of 2-μm diameter, focused with a magnetic quadrupole triplet lens. A variety of irradiation modes have been established for radiation-induced bystander effect, cytoplasm irradiation and so on. In addition, a time-controlled irradiation mode for targeting thick biomaterials has also been established, and this mode has been demonstrated with zebrafish embryos elsewhere [17, 18]. These SPICE performance modes are in routine use and are stable enough to conduct irradiation experiments. SPICE is currently administered as a joint-use research facility for collaborative projects and its beam times are provided for collaborative research.

MATERIALS AND METHODS

Outline of SPICE

The SPICE facility at NIRS is a focused vertical microbeam system designed to target the nuclei of adhesive mammalian cells by irradiation with a defined number of protons [14–16]. It is one of four beamlines at the NIRS electrostatic accelerator facility, which supplies protons and helium ions from the 1.7-MV Tandetron accelerator (Model 4117MC, High Voltage Engineering Europa B.V., the Netherlands) equipped with a duo-plasmatron type ion source (Model 358, High Voltage Engineering Europa B.V., the Netherlands). The other three beamlines are the conventional in-vacuum PIXE line, the in-air PIXE line and the micro-PIXE line for two-dimensional mapping of multielemental distributions [19]. The system for PIXE analysis and the Tandetron accelerator is called PASTA (*P*IXE *A*nalysis *S*ystem and *T*andem *A*ccelerator).

Figure 1 shows a schematic diagram of SPICE with a photograph of the microscope and operation systems. A 3.4-MeV proton beam passes through the microslits, the beam deflector (which acts as a shutter), and then the 90° bending magnet by which the beam direction is changed from horizontal in the micro-PIXE beamline to vertical in the SPICE beam line. In the vertical SPICE beam line, the proton beam is focused to a spot approximately 2 μm in diameter by the slits and quadrupole magnetic lens and then led into air through the exit window of a 200-nm thick silicon nitride film. The proton microbeam passes through the Mylar film of the cell dish that is placed on the micro-positioning stage of the fluorescent microscope and then

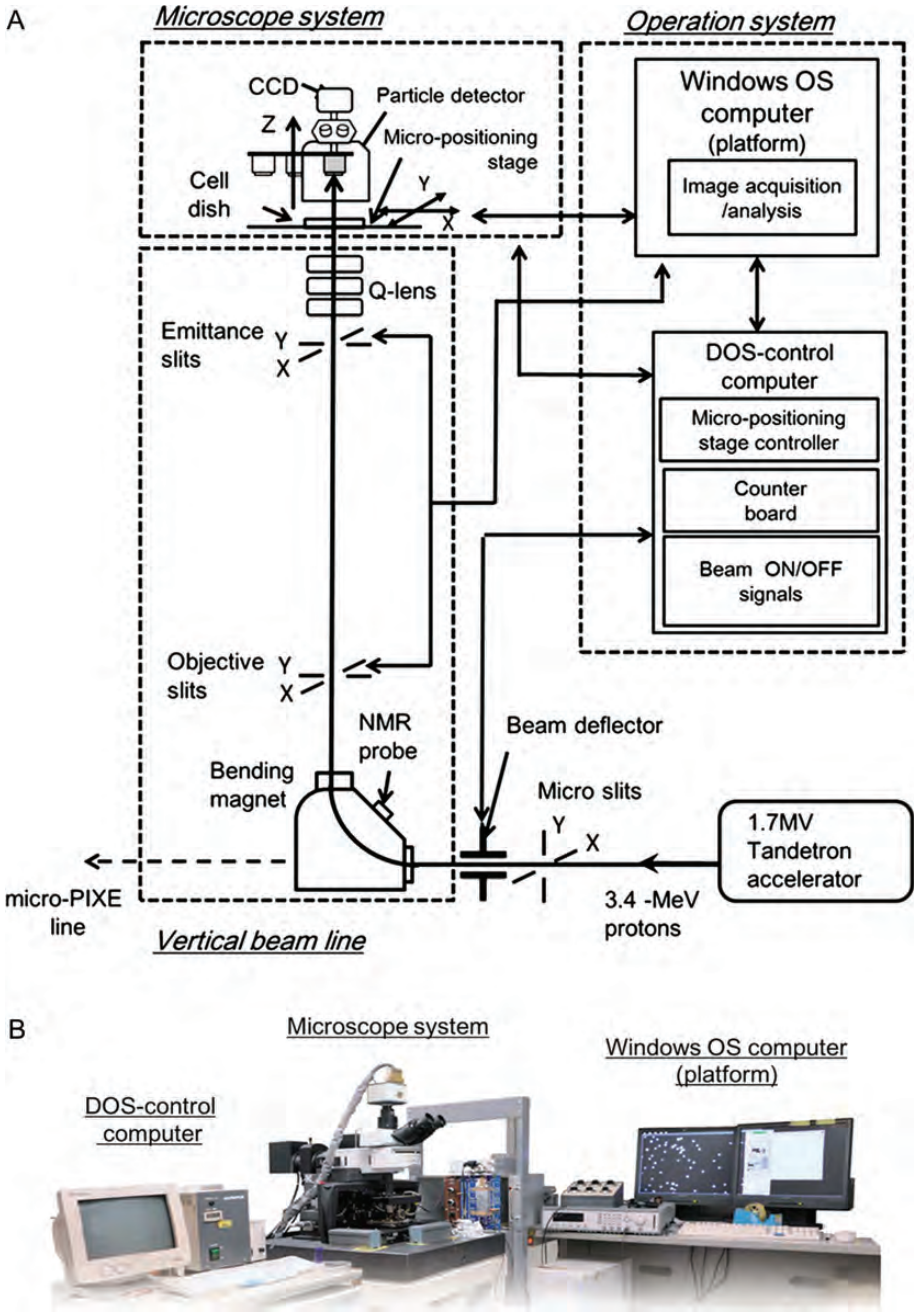

Fig. 1. A schematic diagram (**A**) of the vertical microbeam system for 3.4-MeV proton, SPICE of NIRS, and a photograph (**B**) of the microscope system and the computers of the operation system.

irradiates a cell. After passing through the cells, the protons enter the plastic scintillator of the particle detector mounted on the lens slide unit of the microscope, which is set above the cell dish. The resultant scintillation light is converted into an electric pulse; the number of pulses translates directly into the number of protons that irradiated the cell. When the pulse number reaches a preset value, irradiation is stopped and the cell dish is moved to place another cell in the beam position. All the devices are controlled by an operation system consisting of two computers. The microscope and operation systems are set in an irradiation cabin on a platform with an outer frame that is 4.6 m above the floor. The inner frame is the vertical beam line cradle. In the basement of NIRS, a biological laboratory equipped with benches, incubators, an off-line microscope and other equipment is available for biological experiments, such as sample preparation and bio-assays after microbeam irradiation.

Vertical beam line and beam focusing system

The microslits in front of the beam deflector limit the cross-section of the proton beam, so that it passes through the centre of the bending magnet, and reduce the beam intensity to 1.0×10^4 protons/s for routine irradiation. The fast beam deflector is installed upstream of the bending magnet and is used to switch the beam on and off on demand. It consists of two parallel metal electrodes, 60 mm in length with electrode gaps of 20 mm, which are connected to a pulse generator module (PVM-4210, Directed Energy Inc., CO, USA) providing two simultaneous differential voltage pulses of +950 V and –950 V to each electrode with a pulse rise and fall time of 15 ns. The bending magnet (Takano Giken Co., Ltd, Japan) has a bending radius of 400 mm with a magnetic gap of 32 mm and is driven by a power-supply unit (Ultrastab867-2001, Denmark) with a stability of 10^{-6}. To increase the stability of the magnetic field, a magnetic-field controlling unit (ENC-150NIT; Echo-Electronics Co., Ltd, Japan) with a nuclear magnetic resonance (NMR) probe (Echo-Electronics Co., Ltd, Japan) is employed.

The beam focusing system consists of objective and emittance micrometre-controlled slits (OM10; Oxford Microbeams, Ltd, Oxford, UK) and a monobloc triplet quadrupole magnetic lens (Q-lens) (OM170; Oxford Microbeams, Ltd, UK), which is designed for vertical mounting. The Q-lens focuses the image of the objective slits that are installed just above the bending magnet, and the emittance slits limit the divergence of the beam. These slits are driven by linear actuators (MAS-D23H10; Citizen Chiba Precision Co. Ltd, Japan) with a position resolution of ±3 μm. The distance from the objective to emittance slits is 1810 mm and that to the entrance of the Q-lens is 2750 mm. The distance between the exit of the Q-lens and the focal plane at the Mylar film is 150 mm. With this configuration, the demagnification factors in the X and Y directions, as defined in Fig. 1. are 4.6 and 25, respectively, according to a first-order transport calculation (PBO Lab 2.1.2, Accelsoft Inc., CA, USA) [20]. The Q-lens is equipped with a power supply and a DC current transducer (originally designed by Takano Giken Co., Ltd, Japan), which monitors the applied current and provides feedback to the voltage reference used to generate the demand signal; the stability of the current is 10^{-6}. The upper limit of the beam intensity is set by the shutter speed; thus, the system is routinely adjusted to fix the beam intensity to 1×10^4 protons/s. The size and shape of the focused beam were observed using the fluorescence from a CaF_2 crystal (1 mm thick) set on the Mylar film of the cell dish, and confirmed not to drift within the net microbeam irradiation time (usually 3 h) in a working day.

Figure 2 shows a schematic diagram of the microscope system and associated components. Before reaching the target cell on the Mylar film, the 3.4-MeV proton microbeam traverses the beam exit window, the air gap between the window and the Mylar film, and the Mylar film; the energy of the incident protons decreases to 3.37 MeV and the beam is also broadened. Thus, this distance needs to be as short as possible; the exit window is a 200-nm thick silicon nitride film 1 mm^2 in area (Silson Ltd, UK), which sustains the pressure difference between the vacuum of the beam line and atmospheric pressure. The air gap is the minimum practical distance, 100 μm, which is determined by measuring the focal distance between the top of the window and the bottom of the film using the 20× objective lens of the microscope.

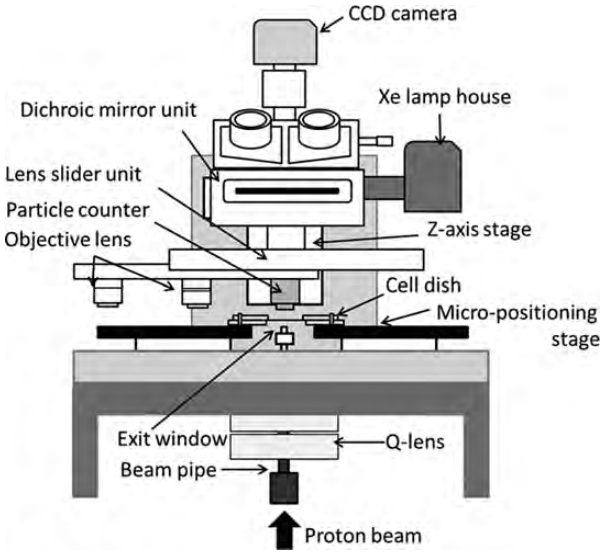

Fig. 2. A schematic diagram of the microscope system and the end of the vertical beam line.

Particle detector and CR-39 plastic track detector

The particle detector is set in an objective lens shaped container, in which a plastic scintillator 1 mm thick with silver deposition on one side (NE102; Ohyo Koken Kogyo Co., Ltd, Japan) is set in front of a compact-size photomultiplier tube (R7400U-03; Hamamatsu Photonics K.K., Japan). The particle detector is mounted on the lens slider unit of the microscope and set above the cell dish during irradiation (see Fig. 2). The scintillation light produced by incident protons is converted to an electrical pulse by the photomultiplier. After low-height signals from the background noise are excluded by a discriminator module (octal discriminator, KN1300; Kaizu Works, Co., Japan), the standard nuclear instrumentation module (NIM) pulse output is fed into a computer-based counter board installed in the DOS-controlled computer, thus counting the number of protons transmitted through the cells. When the number of protons reaches a preset number, the DOS-controlled computer sends a trigger signal to close the shutter and stops

counting 1 ms later. The trigger signal to the pulse generator module for the shutter is transferred by an optical fibre cable to reduce any time delay that may affect the precision of the particle delivery to the target. The exact number of incident protons is controlled by the particle detector and fast beam shutter.

The two-dimensional microbeam profile is detected by a plastic track detector (CR-39, HARZLAS TD-1; Fukuvi Chemical Industry Co., Ltd, Japan) that can record tracks of protons with energies of up to ~ 20 MeV; the detection efficiency of 3-MeV protons is considered to be 100% [21]. A CR-39 disk with a diameter of 15 mm and a thickness of 110 μm, which is shorter than the range of 3.37-MeV protons in the CR-39 (186.56 μm [22]) is adhered to the Mylar surface of the cell dish. After irradiation, the CR-39 disk is etched in 7 M NaOH at 70°C for 2 or 3 h and then observed with a confocal laser microscope (Fluoview1000, Olympus Co., Japan) with a 40× objective lens (NA: 0.95; UPLSAPO 40 × 2, Olympus Co., Japan) over 1024 × 1024 pixels (0.309 μm/pixel) or with a 20× objective lens (NA: 0.75; UPLSAPO 20 ×, Olympus Co., Japan) over 1024 × 1024 pixels (0.623 μm/pixel).

Microscope system

A schematic diagram of the microscope system is shown in Fig. 2 and consists of a fluorescent microscope (BX51; Olympus Co., Japan) equipped with an X–Y stage (Seiko Precision Inc., Japan), lens slider unit (Seiko Precision Inc., Japan), and a Charge Coupled Device (CCD) camera (C4742-95-12ER, ORCA-ER; Hamamatsu Photonics K. K., Japan). The micro-positioning stage is set perpendicular to the proton microbeam and driven by two voice coil motors (TVA3-10; Techno-hands Co., Ltd, Japan) with an 8-mm working distance and an accuracy of 40 nm. The two objective lenses and particle detector are set on the lens slider unit, which is moved by a ceramic motor (HR-2; Nanomotion Ltd, Japan) in the horizontal direction with a resolution better than 0.1 μm. The slider can also be moved in the vertical (beam) direction using a Z-axis stage controlled by an ultrasonic motor (UN30NE; Canon Precision Inc., Japan) to set the lens at the focus position and to bring the particle detector down to the beam exit window. The CCD camera that records the fluorescent images is a high-resolution digital black and white camera with best noise characteristics at substantially high frame rates. A Xe lamp (U-LH75XEAPO; Olympus Co., Japan) and five dichroic mirrors (U-MBF3, U-MWU2, U-MWIBA3, U-MGFPPHQ, U-MWIGA3) are used for the observation of different fluorescence wavelengths, and a halogen lamp (U-LH100L-3; Olympus Co., Japan) is used for positioning the cell dish and confirming the air gap distance. Light exposure from the halogen and Xe lamp can be turned on and off with a mechanical shutter (Sigma Koki Co., Ltd, Japan) controlled by the Windows OS computer.

Cell dish and cell culture

The cell dish for the microbeam irradiation has to satisfy several requirements: first, the dish must be capable of culturing mammalian cells; second, the bottom film of the dish must be as thin as possible so as to keep the divergence of the microbeam to a minimum; and third, the bottom film must have good access on both the lower and upper sides for the beam to pass through the exit window and to the particle detector and objective lens. A photograph and schematic diagram of the cell dish are shown in Fig. 3. The bottom of the dish is a Mylar film (Chemplex Industries, Inc., FL, USA) with a thickness of 2.5 μm, which is the thinnest commercially available, and is stretched so that it is tight and smooth within the jig. The jig consists of three stainless steel parts: a 55 mm × 55 mm square plate 5 mm in thickness with a central hole 33 mm in diameter, a ring with an inner diameter of 33 mm and screws to fix the plate and ring. In addition to the standard cell dish, a smaller dish is prepared for time-lapse observations of the targeted cells in the off-line microscope system, since the cell dish must be put in a small CO_2 incubation chamber (Type-UK; Tokai Hit Co., Ltd, Japan). For the smaller dish, the four corners of the bottom plate are removed, and the inner diameter of the ring is reduced to 24 mm (Fig. 3A; right).

The Mylar film is set 0.5 mm above the bottom of the square plate to prevent the film from attaching to the bench surface during the procedures necessary for pre- and post-

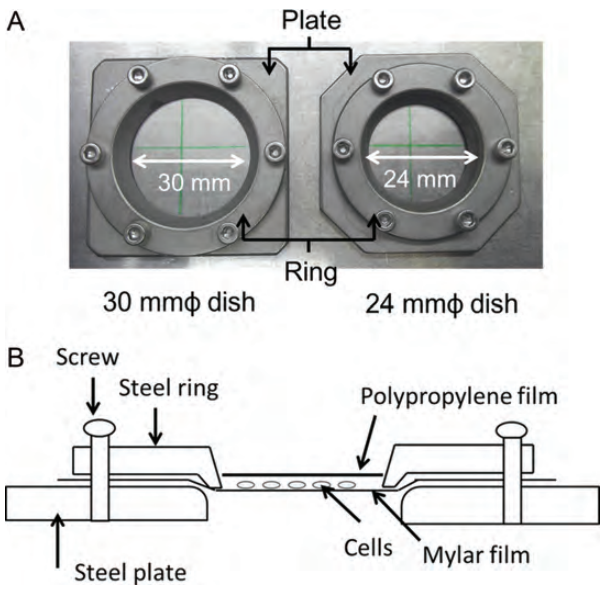

Fig. 3. A top view photograph (**A**) and a schematic diagram in section (**B**) of the two types of cell dishes. The Mylar film on which cells are grown is stretched tight and smooth with tow jigs: the left one has a steel ring of 33 mm inner diameter and the right has an inner diameter of 24 mm; these are referred to as the 33-mm dish and 24-mm dish, respectively.

irradiation and in the case of the dish being placed in other containers for cell culture. The beam exit pipe has an outer diameter of 3 mm, and the distance between the beam exit window and the Mylar surface is set so that the air gap is 100 μm, as mentioned earlier. Since the inner edge of the cell dish and the objective lens limit the movement of the micro-positioning stage, the practical working distance is limited to within a 7 mm × 7 mm area for the 33-mm dish and a 2.5 mm × 2.5 mm area for the 24-mm dish.

Prior to cell culturing, the stainless steel parts of the cell dish were sterilized by an autoclave, and after the dish is assembled, the Mylar film is sterilized by 70% ethanol and UV irradiation. The bottom side of the Mylar film is marked with a cross in the X–Y direction using a permanent marker. The intercept is used as a landmark to define the origin, i.e. (X, Y) = (0, 0), and for later observation of the cells.

For the preliminary experiments, the WI-38 human normal diploid cell line (lung fibroblast, ATCC number: CCL-75) was used. Cells were cultured on the surface of the Mylar film directly or after being coated with 100 ng/ml fibronectin (356008; BD Biosciences, MA, USA) in phosphate buffered saline (PBS). Culturing was performed in an antibiotic-supplemented media (D-MEM with 10% foetal bovine serum (FBS), 2 mM L-Glutamine, 100 U/ml Penicillin and 100 μg/ml Streptomycin) in 5% CO_2 in air at 37°C. An appropriate number of cells for the microbeam irradiation is $3–5 \times 10^5$ cells per 33-mm dish with 2 ml medium or $2–3 \times 10^5$ cells per 24-mm dish with 1 ml medium. The WI-38 cells were cultured in the cell dish the day before irradiation and stained with 1 μM Hoechst 33342 (H342; Dojindo Molecular Technologies, Inc., Japan) in a CO_2 incubator 30 min before irradiation. The toxicity of the fluorescent dye must be confirmed and optimized with each cell line, as has been reported previously [23].

Control system

The control system consists of two computers, a Windows OS computer as a platform and a DOS-controlled computer, and software. The principal connections between the control system and the components of the microbeam system are shown in Fig. 1. The vast majority of the operational features of SPICE are controlled by the Windows OS computer (Pro4700; Seiko Epson Corp., Japan) with software developed in-house. The software controls the experimental procedures automatically including the image processing of the CCD camera images, the movements of the lens slider, Z-axis unit and micro-positioning stage, and the signaling to the beam deflector. The computer-based counter boards for the particle detection are integrated into the DOS-controlled system.

Fluorescent image capturing and cell recognition

Figure 4 shows examples of fluorescent microscope images of the WI-38 cells. Since the 20× objective lens is set on

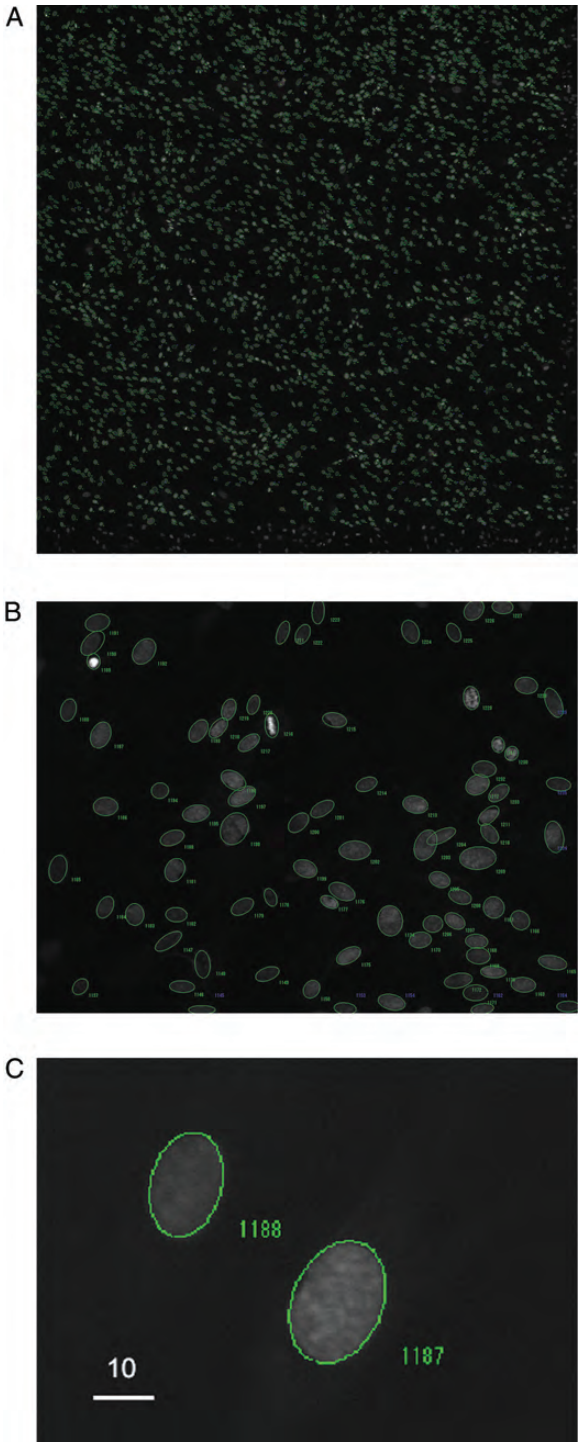

Fig. 4. Fluorescent microscope images of the WI-38 normal human fibroblast cells dyed with Hoechst 33342. (**A**) A microscope image constructed from 6 × 8 single images each 430 μm × 330 μm in size taken with a 20× objective lens. The total image size is 2.58 mm × 2.64 mm. (**B**) An enlarged view of the single image indicated by the rectangle in (A). (**C**) An enlarged view of the two cell nuclei in the white rectangle in (B). The green ellipses define the cell nuclei identified by the recognition software; identification (ID) numbers are also shown for each nucleus. Scale bar sizes are shown in figures in micrometres.

the lens slider unit, a single CCD image covers an area of 430 μm × 330 μm over 1344 × 1024 pixels (Fig. 4B). A larger image can be constructed by tiling several images taken successively by moving the micro-positioning stage in the X and Y directions. The maximum image size constructed from 12 × 16 single images is 5.16 mm × 5.28 mm. Figure 4A shows an example of a tiled image 2.58 mm × 2.64 mm in size constructed from 6 × 8 single images. The single image indicated by the white rectangle is shown in panel B.

Figure 4C shows an enlarged view of the image indicated by the rectangle in panel B. The green ellipses surrounding the bright areas, identified as cell nuclei, are results of the automated recognition software Pit Fit, which was specifically designed to measure the etch pit opening parameters on the CR-39 nuclear track detector [24, 25]. The first step is to set a threshold value for the fluorescent intensity to separate the cells from the background and set upper and lower limit pixels of the object areas to discriminate against objects that are too large or too small. According to these parameters, the X–Y coordinates of the centre of the fluorescence area are calculated based on a least-squares fit to a second order polynomial, $ax^2 + bxy + cy^2 + dx + ey + f = 0$, with the constraint $4ac - b^2 = 1$, which defines the assumed elliptical shape of a cell nucleus. The intersections of the major and minor axes of the fitted ellipses give the (X, Y) coordinates of the centres of the cell nuclei. Figure 4C shows an example image with the fitted ellipses and their identification (ID) numbers. The ID numbers given to each (X, Y) coordinate set together with the corresponding to the cell images are shown on the display of the operation system, and the first set of parameters are adjusted until proper cell recognition is achieved. The final ID numbers, (X, Y) coordinates and cell images are saved to the Windows OS computer as a log file, which can be used at the time of irradiation and for later biological experiments.

Targeting patterns

The default targeting pattern mode is single position irradiation at the centre of the cell nucleus for all nuclei with the same preset number of protons or for each nucleus to be irradiated with a different number of protons. In addition to the default mode, three types of optional targeting modes are provided for a variety of radiobiological studies: a fractional population targeting mode, a multi-position targeting mode for nucleus irradiation and a cytoplasm targeting mode. In the fractional population targeting mode, which is useful for bystander-effect studies, the percentage of irradiated cells among all cells is a set value. The targeted cells are selected randomly from the list of (X, Y) coordinates.

A schematic diagram of the multi-position targeting mode is shown in Fig. 5A. The ellipses represent the cell nuclei, and the solid circles are the automatically calculated central points. The open circles are off-centre positions at a distance of d μm, which can be up to 20 μm. The number of off-centre positions in a nucleus, p, can be set from 1 to 4, and their (X, Y) coordinates are calculated automatically in fixed directions regardless of the direction of the fitted ellipses. For $p = 1$, the position is on the right-hand side of the centre in the X direction; for $p = 2$, the positions are on both sides of the centre in the X direction; for $p = 3$, one position is above the centre in the Y direction and two positions are at angles of ±120° to the Y direction; and for $p = 4$, two positions are at angles of ±45° and two are at angles of ±135° to the X direction. For this mode, all the off-centre positions are irradiated with an option to also irradiate the centre position; thus, a total of eight different patterns are available.

A schematic diagram of the cytoplasm targeting mode is shown in Fig. 5B. The positions indicated by the two open circles are calculated according to a desired off-centre distance of d, which is larger than the major radius. The $+d$ position only or both off-centre positions can be targeted in this mode, with an option to include the centre of the nucleus, giving four different patterns. The fractional population targeting mode can also be used in conjunction with the cytoplasm and multi-position targeting modes.

Time-controlled irradiation for thick biomaterials

Thick biomaterials will be used to denote biological targets thick enough to prevent the 3.37-MeV protons, which have maximum range in water of 180 μm, from entering the particle detector installed above the cell dish and thus preventing a direct count. The number of protons is indirectly estimated by the product of the average number of protons per second and the time width of the beam shutter opening. The time width can be set from 100 μs to 1 s. If the number of protons per second is adjusted to produce the routine intensity of 1×10^4, then the irradiation time for 500 protons is 50 ms with a standard deviation of about 5.4%. Since the number of protons obeys a Poisson distribution, statistical fluctuations are inevitable; that is, the statistical standard deviation is 4.5% (= $(500^{1/2}/500) \times 100$). This means that the standard deviation of the proton intensity is mainly due to this statistical deviation. Stable time-controlled irradiation is achieved due to the stability of the accelerator, bending magnet and vertical beam line.

An example of thick material is zebrafish (*Danio rerio*) embryos, which have a diameter of about 700 μm at a developmental stage of 5 h post-fertilization (hpf). The special setup for holding the zebrafish embryos is described elsewhere [17, 18]. Briefly, to restrict the movement of the embryos, ~17 dechorionated embryos are placed on the surface of the Mylar film and packed into a 3 mm × 3 mm hole of a silicon nitrite plate with 7.5 mm × 7.5 mm frame and a thickness of 200 μm (Silson Ltd). The embryos are

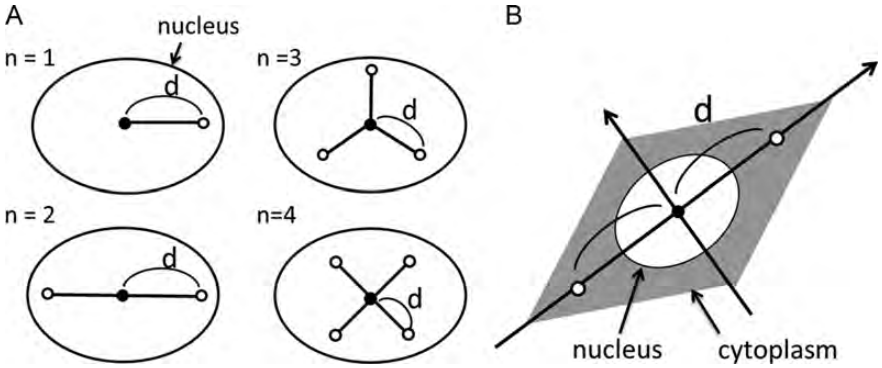

Fig. 5. Schematic diagrams of the optional targeting modes. (**A**) The multi-position targeting mode: the centre of the cell nucleus is shown by a solid circle, and off-centre positions at a distance of d μm (up to 20 μm) are shown by the open circles. The configurations for different numbers of off-centre positions, p (= 1, 2, 3 or 4), are also shown. (**B**) The cytoplasm targeting mode. The two open circles on the major axis are a distance of d from the centre.

placed such that all embryo cells are oriented towards and contacting the Mylar film surface. Images are captured using the 2× objective lens with an image size of 4.3 mm × 3.3 mm, which includes all embryos in the restricted area in a single image. The targeted positions are marked manually on the captured image. The time period for a desired number of protons is estimated by the beam intensity (counts per second) measured using the particle detector prior to the embryo irradiation. The number of protons irradiating the embryos is determined by averaging the counts measured with the same time width of the beam shutter opening before and after sample irradiation.

Visualization of DNA double strand breaks in microbeam irradiated cells

For the visualization of DNA double strand breaks, the irradiated cells were incubated under culture conditions for 30 min before fixation and immunostaining against γ-H2AX, which is known as a marker for DNA double strand breakage [26]. Cells were fixed using 4% paraformaldehyde for 15 min and permeabilized at room temperature in 0.5% Triton X-100 in PBS for 10 min. After cells were washed and blocked (0.2% BSA in PBS) for 1.5 h at 37°C, they were incubated with primary antibodies at 1:500 (Anti-phospho-Histone H2A.X (Ser139) Antibody, clone JBW301, 05-636; Merck Millipore, MA, USA) overnight at 4°C and with secondary antibodies at 1:400 (Alexa Fluor® 488 Goat Anti-Mouse IgG (H + L), A-11001; Molecular Probes, OR, USA) for 1 h.

RESULTS

Beam size measurement and microbeam drawing using CR-39

The beam size was determined by a CR-39 plastic track detector. Figure 6A shows images of the CR-39 detector after irradiation with 1 to 1000 protons at different positions at 50-μm intervals and etching for 2 h. From this image, over 95% of the protons were calculated to be delivered to an area with a diameter smaller than 2 μm for 100 protons per position and to an area with a diameter smaller than 5 μm for 1000 protons per position. In terms of the positional stability, the beam position does not move during the typical 3-h beam time.

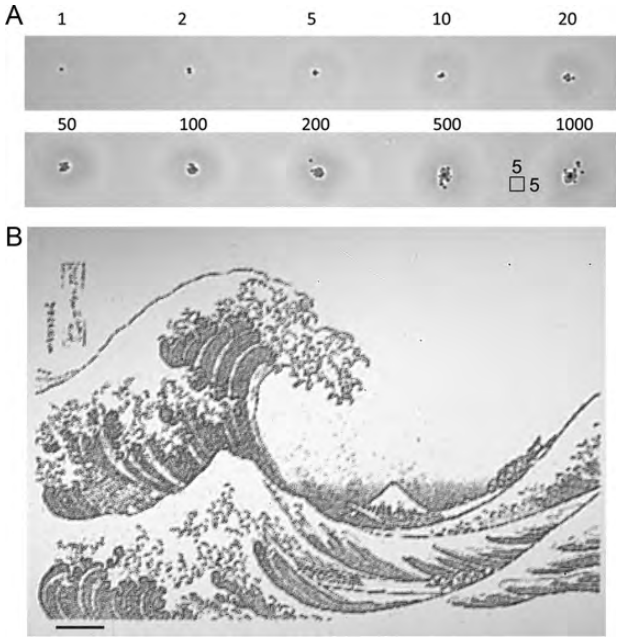

Fig. 6. (**A**) Beam profiles recorded on a CR-39 detector after irradiation with different numbers of protons, as indicated above the images. Square indicates 5 μm × 5 μm size. (**B**) Microbeam drawing of '*The Great Wave off Kanagawa*' (Hokusai) on a CR-39 detector. Scale bar: 100 μm.

Figure 6B shows an image drawn on a CR-39 detector using the microbeam (microbeam drawing). The image is

Hokusai's '*The Great Wave off Kanagawa*'. The image was first converted to 275 × 400 points and an 8-bit grey scale, which was then translated into preset numbers of protons from 0 to 10. The CR-39 plate was irradiated with the microbeam for the preset numbers of protons at 3-μm intervals, and the microbeam drawing had a final size of 825 μm × 1200 μm. Of the 110 000 (= 275 × 400) points, 21 281 points were irradiated by one or more of the 164 314 protons, and the microbeam irradiation was completed within 43 min, meaning that 8.2 positions were irradiated in 1 s.

Proton delivery precision

The dosage precision, which is defined as the percentage of precise irradiations for a preset number of protons, was examined for the single-particle irradiation case. Instead of the cell dish, a thin CR-39 detector was adhered to the surface of the Mylar film, and thus the results of the CR-39 detector were simultaneously obtained with those of the particle detector. The thickness of the CR-39 detector was chosen to be within the range of 80–90 μm so that the energy loss and spatial scattering of the proton beam were similar to those for a cell sample with a thin medium layer and a thin polypropylene film, as determined by an SRIM-2010 calculation [22]. In this way, we can directly compare the results of the particle detector and the CR-39 detector under similar irradiation conditions. The comparison was used to optimize several parameters related to detector efficiency, such as the beam intensity, beam deflector voltage and discrimination level of the particle detector signals.

Figure 7 shows a representative image of a CR-39 detector after irradiation with one proton at 21 × 21 lattice points at 20-μm intervals and subsequent etching for 3 h. There is 1 etch pit at each lattice point except for the 5 lattice points indicated by the crosses where there is either no etch pit (2 points) or 2 etch pits (3 points). A total of 4410 points from 10 images like those of Fig. 7 were analysed: 31 points had no etch pit, 4366 points had 1 etch pit, 12 points had 2 etch pits, 1 point had 3 etch pits and no points had 4 or more etch pits. The dosage precision was 99.00% (= (4366/4410) ×100). Table 1 summarizes the number of lattice points with 0, 1, 2 and 3 etch pits of the CR-39 and the number of lattice points classified according to the particle detector counts (1, 2 and 3) that were simultaneous measured. The discrepancy between the number of CR-39 etch pits and the counts of the particle detector is considered to be caused by false counts due to noise except for the lattice point with 2 etch pits and 1 count, which may be explained by the piling up of two proton pulses so close in time that the pulses were recognized as a single big pulse. The particle detector correctly counts one proton for 4321 positions and two protons for 11 positions. This gives a counting accuracy of 98.23%, which is the probability of accurate detection.

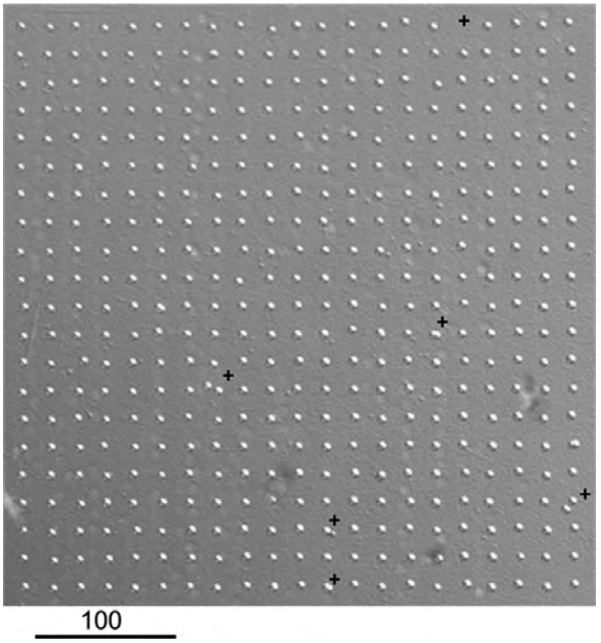

Fig. 7. (**A**) 21 × 21 array of etch pits at 20-μm intervals on a CR-39 detector after irradiation at each point with a single proton and subsequent etching for 3 h. The six crosses indicate points at which there is no etch pit or two etch pits. Scale bar: 100 μm.

Microbeam-induced DNA double-strand breaks in a targeted mammalian cell

To determine whether the microbeam irradiation has sufficient accuracy for mammalian cell studies, DNA double-strand breaks induced in the cell nuclei by irradiation were visualized using the γ-H2AX immuno-staining technique [26]. Figure 8A shows an example image of the WI-38 cells irradiated at the centre of the nucleus with 200 protons and subsequently immune-stained with anti-γ-H2AX antibody and a Alexa 488 secondary antibody. First, the efficiency of the automatic cell recognition program was tested. A total of 3061 cells was confirmed by manual scoring in an irradiation area, but only 2982 cells were automatically recognized by the analysing software using optimized parameters; thus, 97.4% of the cells were successfully recognized. The missing portion was mainly due to overlapping cells, which were sometimes recognized successfully as two single cells but occasionally falsely identified as a large dust particle.

Within the irradiated area, there were 2892 γ-H2AX positive cells, which show a clear γ-H2AX fluorescent spot in the nuclei. The immune-fluorescence positive cells accounted for 97.0% of the targeted cells and 94.5% of the total cells. The difference in the percentages was mainly due to the detachment of cells during the irradiation and immuno-staining procedures in addition to a few cells that showed a highly positive response to γ-H2AX but did not show a clear fluorescent spot and were thus excluded from the count.

Table 1. Numbers of lattice points with zero, one and two etch pits of CR-39 with numbers of lattice points classified according to the particle detector counts (1, 2 and 3) simultaneous measured after the irradiation of the CR-39 detector at each lattice point with the preset number of protons, $n = 1$

	Number of lattice points					
Number of etch pits per lattice point	**0**	**1**	**2**	**3**	**Subtotal**	**%**
Particle detector count[a]						
1	31	4321	1	0	4353	98.71
2	0	44	11	1	56	1.27
3	0	1	0	0	1	0.02
Subtotal	31	4366	12	1	4410	
%[b]	0.70	99.00	0.27	0.02		

Protons penetrated through the CR-39 detector with 80–90 μm thickness and then hit the plastic scintillator of the particle detector. The total number of lattice points was 4410 coming from 10 images with 21 × 21 lattice points.

[a] Since the operation system sent the close signal to the shutter after the particle detector counted one for the irradiation with the preset number of protons, $n = 1$, it was impossible for the number of counts of the particle detector to be 0.

[b] The sum of the percentages was not 100 owing to a rounding-off error.

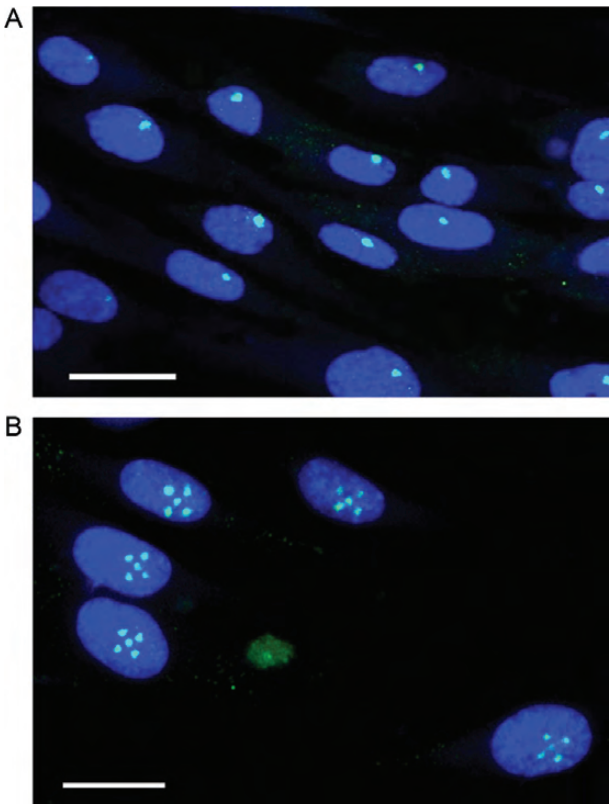

Fig. 8. Detection of microbeam-induced DNA double-strand breaks in targeted WI-38 cells in which the nuclei were stained with Hoechst 33342 (blue) and immuno-stained against γ-H2AX (green). (**A**) Cell nuclei irradiated at one position with 200 protons. (**B**) Cell nuclei irradiated at five different positions with 200 protons per position. Scale bar: 20 μm.

Figure 8B shows an example of the multi-position targeting mode with $p = 4$ and an off-set distance of 3 μm with the central position irradiation included; this results in a total of five irradiated positions. Five distinct fluorescent spots shown in Fig 8B were observed in the five nuclei in this figure, indicating that the double strand break induction did not diverge over the 2-μm diameter of the microbeam. Similar images to Fig. 8B have already been reported using the heavy ion microbeam of GSI, Darmstadt, after immuno-staining of cell nuclei against 53BP1 or γ-H2AX [27, 28]. It should be noted that heavy ions are advantageous for these experiments because they are less readily scattered, and particle detection is less problematic in the microbeam technique. In contrast to heavy ions, protons are easily scattered in materials, and therefore, the beam exit window, air gap and cell cultured film all critically broaden the size of the microbeam. These physical characteristics have also been mentioned by others [30]. Regardless of the critical disadvantages of the proton beam, we demonstrated a 2-μm beam size and a high targeting resolution equivalent to those of heavy ion microbeams.

DISCUSSION

Protons of 3.4 MeV

Since the linear energy transfer (LET) is one of the important values that characterize radiations, LET in water of the 3.37-MeV protons was calculated using SRIM-2010 as 11.0 keV/μm [22]. This LET value is the same as that for 1 keV electrons with a 53-nm range [31], and thus the results from the 3.4-MeV proton microbeam can be considered relevant for simulating biological effects by low LET radiations, with respect to LET. The LET of electrons increases to a maximum of 30 keV/μm at 0.1 keV and then decreases with increasing energy. The maximum LET of protons is 82.6 keV/μm at 80 keV, but the LET increases

from 11.0 keV/μm at 3.4 MeV to 30 keV/μm at 0.8 MeV, and over the maximum decreases to 30 keV/μm at 5 keV. Thus, protons with an energy range of 3.4–0.8 MeV and those below 5 keV have similar LETs at electron track ends. This can be considered as the most unique and significant property of microbeam-applied radiation biology with the proton microbeam system.

In terms of the absorbed dose, the passage of a 3.4-MeV proton through a cell nucleus with an assumed cross-section of 100 μm^2 gives an estimated dose of 17.6 mGy per proton with an LET in water of 11 keV/μm; the absorbed dose is proportional to the LET, inversely proportional to the cross-sectional area and independent of the thickness of the nucleus if the change in the LET during passage through the nucleus is neglected. The cell geometries of WI-38 cells were measured, which were prepared exactly as those in Fig. 8 except for the cytoplasm, which was fluorescently dyed with 5 μM Cell Tracker Orange (C2927; Molecular Probes, OR, USA) to measure the whole-cell area, and visualized with a confocal laser microscope (Fluoview1000; Olympus Co., Japan). The maximum thickness, cell nucleus area and cell area, measured for 250 cells, were 4.4 ± 1.8 μm, 230 ± 52 μm^2 and 380 ± 82 μm^2, respectively. Thus, the dose for the WI-38 cell and its nucleus can be estimated as 7.6 mGy and 4.6 mGy per single proton traversal with a LET of 11 keV/μm, on the assumption that LET does not change appreciably thorough the cell thickness of 4.4 μm, which can be considered to be a relevant value due to the very small thickness of the cell. From this estimation, SPICE is sufficient in delivering a precise dose to the desired site in the cell from a low dose of several milligrays to up to several grays to several thousand cells in the limited experimental time. Therefore, studies of the distinctive biological effects reported in the low-dose region below 200 mGy, such as hyper-radiosensitivity and other phenomena [23, 32, 33], are practicable with a sufficient statistical targeted cell population number using SPICE. However, it should be kept in mind that these calculations of absorbed dose are superficial, because the cross-sectional area cannot be determined uniquely, for example, if the cross-sectional area is assumed to be 3.14 μm^2 corresponding to the area of the microbeam diameter of 2 μm, which is 8.26×10^{-3} (= 3.14 μm^2/380 μm^2) of WI38 cells and the absorbed dose becomes (4.6 mGy × 121.02 =) 557 mGy.

Performance and overall evaluation

The 2-μm diameter beam size enables us to irradiate the nucleus or cytoplasm of a single mammalian cell, and the number of protons irradiating a single nucleus can be controlled to be one to several thousand with a precision of 99%. Furthermore, SPICE is also convenient and stable. All procedures are controlled automatically by the operation system except for setting the preset number of protons during the standard microbeam irradiation targeting monolayer cells. This may be quite convenient for radiation biologists who are not familiar with microbeam experiments but also very time consuming. For thick biomaterials, such as the zebrafish embryos, a standard microbeam protocol was also established [18, 19]. SPICE provides a stable microbeam for 3 h, and under the standard irradiation protocol conditions, 3000 cells in a cell dish can be irradiated within 15 min, meaning that 12 dishes can be irradiated in 3 h. Since 2009, SPICE has been administrated as a 'joint-use facility for collaborative research', and thus researchers outside NIRS can apply for beam time of SPICE after their research proposals are approved. In 2010, SPICE provided 80 days of 3 h beam time slots a day to external users.

Future improvements

In each nucleus of the cells in Fig. 8A there is a single γ-H2AX fluorescent spot corresponding to the double strand breaks induced by the microbeam. The fluorescent spots, however, are shifted slightly away from the centre of the cell nuclei. In addition, in the cells in Fig. 8B, the five fluorescent spots show an apparent deviation from the centre to the same extent towards the lower right. A few cells in other images also had fewer than five fluorescent spots, indicating that the centre of the nuclei were not targeted accurately. The targeting accuracy is affected mainly by four factors: (i) the positional stability of the microbeam; (ii) the accuracy of the micro-positioning stage; (iii) calibration error of the pixel size in the obtained microscopic images, which were used to calculate the (X, Y) coordinates of each cell nucleus; and (iv) the difference between the real and calculated position due to lens distortions. The first two factors can be considered to be negligible owing to the beam stability discussed earlier, and the micro-positioning stage has an accuracy of 40 nm, which is sufficient for these measurements. Accurate calibration of the microscope image and the stage movement is necessary to achieve a targeting accuracy below 2 μm. The calibration error of the pixel size may need to be improved further for large area irradiation. Moreover, the microscope image of the beam spot and the cells may shifted due to various refraction effects, and the effects of focusing and illumination can give rise to targeting errors of 1 μm or more. The difference between the true and apparent positions becomes substantial when the cells or the beam are off axis [33, 34]. Additional analysis software for calculating the targeting position, including these calibration procedures, is under development to improve the targeting accuracy. Moreover, higher throughputs are still desired for studies of radiation induced mutagenic and oncogenic endpoints where yields are ~10^{-4}, and SPICE is now under consideration for improvement on irradiation speed by beam-scanning mode.

ACKNOWLEDGEMENTS

T.K. would like to thank Professor K. N. Yu at the City University of Hong Kong (CUHK), Dr B. N. Pandey at the Bhaba Atomic Research Centre and Dr J. Wang at the Chinese Academy of Sciences for critical reading of the manuscript. The authors would like to thank Ms V. W. Y. Choi and Ms C. Y. P. Ng at CUHK for wonderful discussions and fruitful advice during this work.

REFERENCES

1. Prise KM, Schettino G. Microbeams in radiation biology: review and critical comparison. *Radiat Prot Dosimetry* 2011;**143**:335–9.
2. Hei T, Zou H, Chai Y *et al*. Radiation induced non-targeted response: mechanism and potential clinical implications. *Curr Mol Pharmacol* 2011;**4**:96–105.
3. Zirkle RE, Bloom W. Irradiation of parts of individual cells. *Science* 1953;**117**:487–93.
4. Folkard M, Vojnovic B, Prise KM. A charged-particle microbeam: I. Development of an experimental system for targeting cells individually with counted particles. *Int J Radiat Biol* 1997;**72**:375–85.
5. Folkard MB, Vojnovic KJ, Hollis AG *et al*. A charged-particle microbeam: II. A single-particle micro-collimation and detection system. *Int J Radiat Biol* 1997;**72**:387–95.
6. Randers-Pehrson G, Geard CR, Johnson G *et al*. The Columbia University single-ion microbeam. *Radiat Res* 2001;**156**:210–14.
7. Randers-Pehrson G, Johnson GW, Marino SA *et al*. The Columbia University sub-micron charged particle beam. *Nucl Instrum Methods Phys Res, Sec A* 2009;**609**:294–9.
8. Bigelow A, Garty G, Funayama T *et al*. Expanding the question-answering potential of single-cell microbeams at RARAF, USA. *J Radiat Res* 2009;**50**:A21–A28.
9. Gerardi S. Ionizing radiation microbeam facilities for radiobiological studies in Europe. *J Radiat Res* 2009;**50**:A13–A20.
10. Kobayashi Y, Funayama T, Hamada N *et al*. Microbeam irradiation facilities for radiobiology in Japan and China. *J Radiat Res* 2009;**50**:A29–A47.
11. Wang XF, Li JQ, Wang JZ *et al*. Current progress of the biological single-ion microbeam at FUDAN. *Radiat Environ Biophy* 2011;**50**:353–64.
12. Greif KD, Grede HJ, Frankenberger D *et al*. The PTB single ion microbeam for irradiation of living cells. *Nucl Instrum Methods Phys Res, Sec B* 2004;**217**:505–12.
13. Merchant MJ, Jeynes JCG, Grime GW *et al*. A focused scanning vertical beam for charged particle irradiation of living cells with single counted particles. *Radiat Res* 2012;**178**: 182–90.
14. Yamaguchi H, Sato Y, Imaseki H *et al*. Single particle irradiation system to cell (SPICE) at NIRS. *Nucl Instrum Methods Phys Res, Sec B* 2003;**267**:2171–5.
15. Imaseki H, Ishikawa T, Iso H *et al*. Progress report of the single particle irradiation system to cell (SPICE). *Nucl Instrum Methods Phys Res, Sect B* 2007;**260**:81–4.
16. Konishi T, Ishikawa T, Iso H *et al*. Biological studies using mammalian cell lines and the current status of the microbeam irradiation system, SPICE. *Nucl Instrum Methods Phys Res, Sect B* 2009;**267**:2171–5.
17. Choi VWY, Konishi T, Oikawa M *et al*. Adaptive response in zebrafish embryos induced using microbeam protons as priming dose and X-ray photons as challenging dose. *J Radiat Res* 2010;**51**:657–64.
18. Choi VWY, Yum EHW, Konishi T *et al*. Triphasic low-dose response in zebrafish embryos irradiated by microbeam protons. *J Radiat Res* 2012;**53**:475–81.
19. Imaseki H, Yukawa M. Introduction of PIXE analysis system in NIRS. *Int J PIXE* 2000;**10**:77–90.
20. Crandall KR, Rustoi DP. 'TRACE 3-D Documentation', LA-UR-97-886, Los Alamos, 1997; PBO Lab by AccelSoft Inc., v. 2.1.2, 2006, http://www.ghga.com/accelsoft. (10 December 2011, date last accessed).
21. Ogura K, Hattori T, Asano M *et al*. Proton response of high sensitivity CR-39 copolymer. *Radiat Meas* 1997;**28**:197–200.
22. Ziegler JF, Ziegler MD, Biersack JP. SRIM – the stopping and range of ions in matter. *Nucl Instrum Methods Phys Res, Sect B* 2010;**268**:1818–23.
23. Schettino G, Folkard M, Prise KM *et al*. Low-dose hypersensitivity in Chinese hamster V79 cells targeted with counted protons using a charged-particle microbeam. *Radiat Res* 2001;**156**:526–34.
24. Yasuda N, Namiki K, Honma Y *et al*. Development of a high speed imaging microscope and new software for nuclear track detector analysis. *Radiat Meas* 2005;**40**:311–15.
25. Yasuda N, Kodaira S, Kurano M *et al*. High speed microscope for large scale ultra heavy nuclei search using solid state track detector. *J Phys Soc Jpn* 2009;**78**:A142–A145.
26. Rogakou EP, Pilch DR, Orr AH *et al*. DNA double-stranded breaks induce histone H2AX phosphorylation on serine 139. *J Biol Chem* 1998;**273**:5858–68.
27. Heiss M, Fischer BE, Jakob B *et al*. Targeted irradiation of mammalian cells using a heavy-ion microprobe. *Radiat Res* 2006;**65**:231–9.
28. Voss KO, Fournier C, Taucher-Scholz G. Heavy ion microprobes: a unique tool for bystander research and other radiobiological applications. *New J Phys* 2008;**10**:075011.
29. Folkard M, Prise KM, Grime G *et al*. The use of microbeams to investigate radiation damage in living cells. *App Radiat Isot* 2009;**67**:436–9.
30. ICRU Report 16. *Linear Energy Transfer*. Washington DC: International Commission on Radiation Units and Measurements, 1980.
31. Gerardi S, Galeazzi G, Cherubini R. Single-ion microbeam as a tool for low-dose radiation effects investigations. *J Phys: Conf Ser* 2006;**41**:282–7.
32. Nuta O, Darroudi F. The impact of the bystander effect on the low-dose hypersensitivity phenomenon. *Radiat Environ Biophys* 2008;**47**:265–74.
33. Fischer BE, Heiss M, Cholewa M. About the art to shoot with single ions. *Nucl Instrum Methods Phys Res, Sect B* 2003;**210**:285–91.
34. Fisher BE. Pitfalls in targeted irradiations of biological cells using an ion microprobe. Why a small beam spot is not sufficient for success. *J Radiat Res* 2009;**50**:A106.